Machine learning classification GEOs using spectral data

Xin C. Yee[1], Phan D. Dao[2], David M. Strong[3], Charles J. Wetterer[4], Benjamin Roth[5], and Francis K. Chun[5]

[1]*Mechanical and Aerospace Engineering, University of Colorado*

[2]*Applied Optimization*

[3]*Strong EO Imaging, Inc.*

[4]*KBR*

[5]*Department of Physics and Meteorology , U.S. Air Force Academy*

1 Abstract

The United States Air Force Academy (USAFA) operates the Falcon Telescope Network (FTN) to support its research program in the Space Situational Awareness (SSA) utility of satellite optical signatures and its mission to train USAFA cadets. The FTN sensors are test beds for developing measurement techniques and collecting photometric, multispectral and polarimetric data. Operated in campaign mode, the system collects data to support the development of techniques to characterize space objects using multi-modal signatures. Specifically, the sensors are equipped with diffraction grating elements to operate as slit- less spectrographs and collect the signatures analyzed in this paper. In this project, we applied dimension reduction and classification techniques on spectroscopic data of geosynchronous

orbit satellites (GEOS) collected using slitless spectroscopy from the USAFA 16-inch and a 20-inch Ritchey-Chretien Falcon telescope. We applied both unsupervised and supervised techniques (limiting spectral resolution, principal component analysis, nearest neighbor classification and support vector machine) to analyze the spectroscopic data. We showed that using only spectroscopic data collected from five nights, we were able to discriminate between 20 different satellites with an approximately 49% accuracy. We showed using a learning curve that the classification accuracy can increase significantly once we collect more spectroscopic data from different nights.

2 Introduction

The expanding number of satellites and space debris contribute to space congestion and elevate the need for SSA. Tracking and identifying techniques are needed to provide SSA for both the United States Space Force and Air Force in this new war fighting domain. Low-earth orbit (LEO) and geosynchronous orbits (GEO) are of specific interest due to the number of satellites that are within these regions of space. A form of surveillance in this domain is through the use of optical telescopes. Spatially resolved images of satellites provide a great assessment of capability and function; however, telescopes with this ability are not always readily available. Satellites in GEO vary in size and present a challenge for resolved imagery when a satellite's size is small compared to the distance. In this paper, we applied dimension reduction and classification techniques on spectroscopic data of GEOS collected using slitless spectroscopy from the USAFA 16-inch and 20-inch Ritchey-Chrétien (RC) Falcon telescope [1]. We applied both unsupervised and supervised techniques (limiting spectral resolution, principal component analysis, nearest neighbor classification and support vector machine, ensemble learning) to analyze the spectroscopic data. This paper presents results of applying machine learning techniques to satellite spectra obtained using transmission gratings.

3 Experimental and Sensor Details

Two USAFA telescopes were used in this study, a 16-inch, f/8.2 RC telescope on the USAFA campus (USAFA-16) and a 20-inch, f/8 RC Falcon telescope on the campus of Northeastern Junior College located in Sterling, Colorado (NJC-Falcon). Both telescopes were outfit with the same 100-lines-per-millimeter transmission grating and nearly identical CCD cameras. The fields-of-view were similar, 13 arcmin for USAFA-16 and 11 arcmin for NJC-Falcon. Figure 1 shows pictures of the two telescopes and a Colorado state map depicting the baseline distance of 289 kilometers between them. The latitude and longitude of the two telescopes are 390 N, -1050 W for USAFA-16 and 410 N and -1030 W for NJC-Falcon. Their nearly equal latitudes, at least to the nearest integer, will allow us to compare features in a satellite's optical signature driven primarily from longitudinal differences. Table 1 presents information on the two telescopes, their respective cameras, and filters used for our observations. Additional information on the systems used and their calibration can be found in [2] and [3].

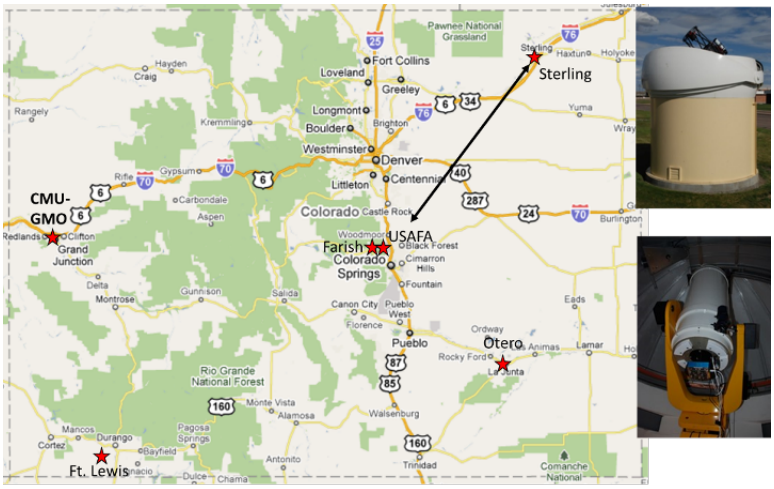

Figure 1: Pictures and location of the two telescopes used in this study: NJC-Falcon located at Northeastern Junior College near Sterling Colorado (top right picture) and the USAFA-16 located at the USAFA campus in Colorado Springs (bottom right picture). The baseline distance between the two telescopes is 289 kilometers and primarily in longitude. Four other Falcon telescopes in Colorado are indicated by red stars.

The majority of light that comes from satellites is attributed to sunlight reflecting off the

Telescope	Camera	Plate Scale (asec px)	Filters
DFM Engineering f/8.2, 0.4-meter (USAFA-16)	Apogee Alta U47	0.80	100 lines/mm Diffraction Grating
Officina Stellare ProRC-500, f/8, 0.5-meter (NJC-Falcon)	Apogee Alta F47	0.65	100 lines/mm Diffraction Grating

Table 1: Characteristics of the telescopes, cameras, and filters used in this study.

various surfaces as shown in Figure 2. As the reflected light passes through the diffraction grating prior to the camera's focal plane, it results in an interference pattern as shown in Figure 2. The zeroth order is the central bright spot that passes straight through to the focal plane and remains a point source, whereas the first order corresponds to that portion that diffracts equally to both sides of the zero-order. However, a diffraction grating can be manufactured such that the majority of the incident light is preferentially diffracted to one side of the zero-order compared to the opposite side. Figure 3 shows an example of a transmission grating image taken the USAFA-16 telescope.

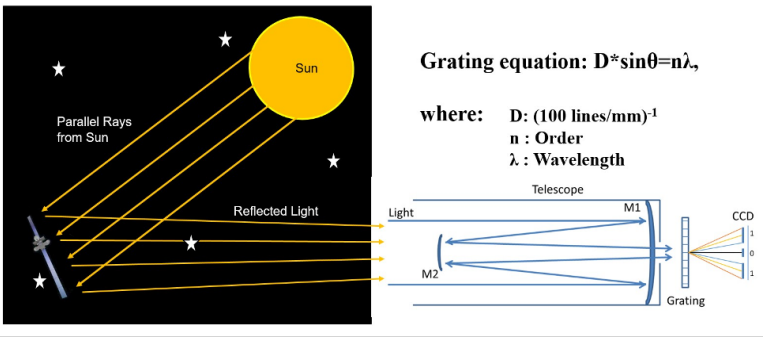

Figure 2: Image shows the imaging scenario between the sun, the satellite, and the observer. Light reflects off the satellite, goes through the telescope where it passes through the diffraction grating. The light is then spread out onto the focal plane based on the grating equation.

Observations are made of the satellites around the equinox, during which time, glints are more likely to occur resulting in very bright reflections. These glints occur when the angle of incidence equals the angle of reflection towards the observer resulting in the brightest

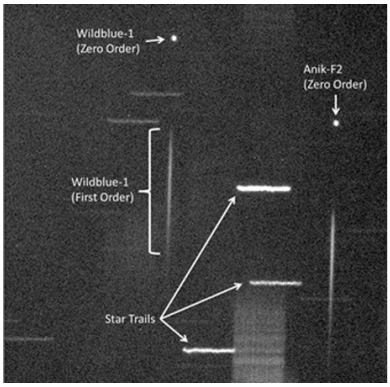

Figure 3: Resulting image taken by the USAFA-16 telescope.

reflections observed. Given the size of the extended light source, the sun, the size of the peak glint produced on the ground is approximately 17 km wide. This assumes a simple model of the satellite as a 2m by 40m plane mirror at GEO orbit. Outside of the peak glint, the intensity of the glint falls off similar to a triangular function. These approximations flow from basic geometric ray tracing. The spot size of the solar reflection on the ground explains some of the varying magnitude of the measured glints throughout the year as a function of the location of the ground observatory. Variations due to ground location will be studied in later projects.

3.1 Data information

The raw spectral data consists of spectral measurements of reflectance intensities measured in counts per second over the visible spectrum ranging from 380 nm - 880nm. The total number of wavelengths measured is 501. The raw data set consists of 594 spectra measurements from 20 satellites for five nights during the Glint season. For each night and each satellite, a number from four to ten spectral measurements are taken with varying time intervals. There is an exception, the satellite MexSat was not observed on the night of August 11, 2022. Table 3.1.1 shows the number spectral measurements collected for each satellites on each night. Figure 4 shows examples of the five spectral measurements for AMC15 and

AnikF1R satellite for the night of August 11th, 2022.

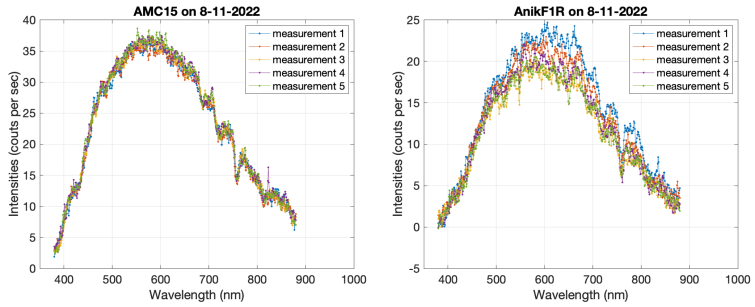

Figure 4: An example of the spectral data for the AMC15 and AnikF1R satellites on August 11th, 2022.

3.1.1 Data preprocessing

To ensure that we have a representative spectral measurement for each satellite, we average over all spectra measurements collected for each satellite per night; this results in a single averaged spectra for each satellite per night. After the averaging, we are left with 99 data points for classification training and testing (i.e. 20 satellites for five nights, with the exception of one missing data point for the MexSat satellite for one night). In addition, we normalized the area under the spectra intensities over the wavelengths to 1 to remove the effects of the different telescopes. Figure 5 shows examples of the averaged and normalized spectra for AMC15 and AnikF1R satellite for the night of August 11th, 2022.

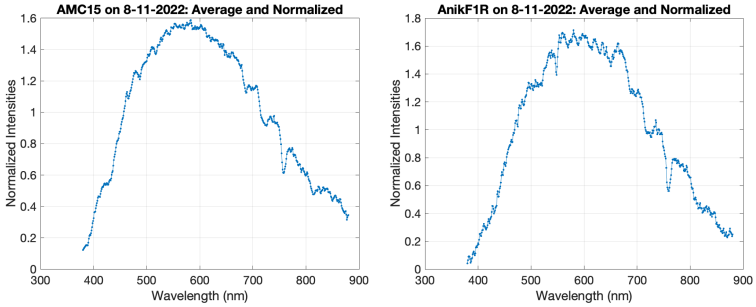

Figure 5: An example of the spectral data for the AMC15 and AnikF1R satellites on August 11th, 2022.

Dates / Sat. Names	8-11-2022	8-13-2022	8-24-2022	8-25-2022	8-28-2022
AMC15	5	5	5	10	5
AnikF1R	5	5	5	10	5
AnikF2	4	5	5	10	5
AnikG1	5	5	5	10	5
DTV10	5	5	5	10	5
DTV12	5	5	5	10	5
DTV14	5	5	5	10	5
DTV15	5	5	5	10	5
Echostar10	5	5	5	10	5
Echostar11	5	5	5	10	5
Echostar17	5	5	5	10	5
Galaxy16	5	5	5	10	5
Inmarsat4F3	5	5	5	10	5
MexSat	0	5	5	10	5
Nimiq2	5	5	5	10	5
SES3	5	5	5	10	5
SES11	5	5	5	10	5
Skyterra1	5	5	5	10	5
Spaceway3	5	5	5	10	5
WildBlue	5	5	5	10	5

Table 2: Number of spectral measurements collected for each satellite for each night of observation.

4 Computational Methods

4.1 Dimension reduction and classification

Below, we briefly summarize the dimension reduction and classification methods used in this work to analyze spectral data from the USAFA 16-in telescope.

Principal component analysis (PCA) is an unsupervised dimension reduction method first introduced in 1901 by Karl Pearson [4]. It finds principal components that maximize the variance of the input data to build a hierarchical coordinate system. Given an input data matrix X, PCA projects the data over a set of orthogonal directions sorted by their contribution to the variance of the input data. The variance matrix of the data is defined by $X^T X$. The eigenvalues and eigenvectors of the variance matrix can be found. The r leading principal components are r eigenvectors with the largest eigenvalues.

For classifying between the different satellites, we used two different classification methods: K-nearest neighbor classification [5] and support vector machine (SVM) [6]. K-nearest neighbor classifies the unknown data by counting the classes of its K nearest neighbors. The class that corresponds to the most number of neighbors is the class for the unknown data. SVM seeks to find a hyperplane that best linearly separates the different classes of data. In the event that the data is not linearly separable, SVM uses two techniques to balance between misclassification of the data and linear separability.

1. Soft margin: this technique broadens the width of hyperplane to allow for misclassification of some points but still keeping most of the points separated. The wider the hyperplane, the more misclassification SVM will allow.

2. Nonlinear transformation of the data: not all the data points are linearly separable. However, by lifting the data to high dimensions through a kernel trick can cause the data to be linearly separable. The common kernels used in SVM are radial basis functions, polynomial kernels and Sigmoid kernel.

4.2 Dimensionality reduction by limiting spectral resolution

This approach starts with calculating the normalized spectral reflectance curve for each spectroscopic signature. We started with the exoatmospheric count which has been scaled to the solar analog and normalized over all wavelengths. The normalization effectively removes the dependence on brightness (object's size, material albedo, and distance). The second preprocessing step is to smooth out the spectrum to a fixed spectral resolution dl/l of 40, a conservative lower bound of the achievable resolutions. The choice of a fixed spectral resolution ensures that any processed spectroscopic signatures have a fixed spectral resolution. In a slit-less spectrum, the spectral resolution depends on the blur spot or the seeing condition at the time of observation. Reducing all measured spectra to a common resolution would remove the variance caused by atmospheric seeing conditions. The processed spectrum is then sampled at 50 equally spaced wavelengths. Figure 6 shows the reduction of spectral signature to produce the 50D signatures used for classification. Machine classification is based on the comparison of signatures. The use of resolution-limited spectral signatures which is a processed copy of the spectroscopic signature itself gives the analysts the opportunity to inspect the signatures in their native form and evaluate the decision of the classifier.

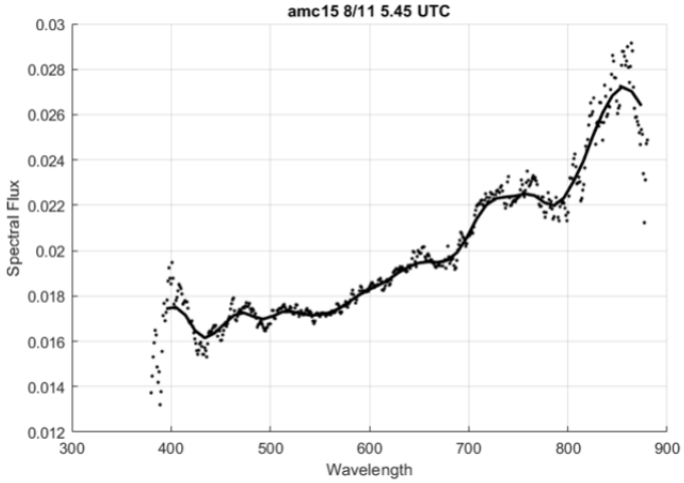

Figure 6: Solar analog scaled and normalized flux and spectral signature with limited resolution (solid line).

5 Results

5.1 Classification of 20 satellites using PCA

To assess the classification accuracy of our machine learning model, we split the spectral data of the 20 satellites from 5 nights into 75% training data and 25% testing data. The testing data is completely unseen by the machine learning model; the training data is used to train the machine learning model using either K-nearest neighbor classification or support vector machine classification. The trained machine learning classification model is used to predict the satellite label of the test data. The accuracy of the prediction is computed using the measure:

$$\text{accuracy} = \frac{\#\text{True positive} + \#\text{True negative}}{\text{Total \# test data}}$$

To ensure that the splitting of testing and training data represents a generalized performance of the classification model, we randomly repeat the training and test split of the data 10 times. For each training-testing split of the data, we train the machine learning model using the training data (75%) and evaluate the accuracy of the machine learning model using the test data (25%). The final accuracy is given as an average over all 10 rounds of train-test split. We compute the average accuracy of the classification model using $1 - 10$ PCA dimension to see the affect of increasing PCA dimensions on classification accuracy.

Figure 7 and 8 show the average accuracy on the test data as a function of the number of PCA components using K-nearest neighbor classification and support vector machine classification.

The K-nearest neighbor classification uses 1 nearest-neighbors to classify the test data. The support vector classification uses a linear kernel with $C = 1.0$.

We can see that average test accuracy maxes out at 15 PCA components with approximately 48.6% test accuracy. The support vector classification shows a slightly worse accuracy at 48.2% at 14 PCA components. The plateauing of the test acurracy as the PCA dimension increases indicates that we have included sufficient PCA components that capture most

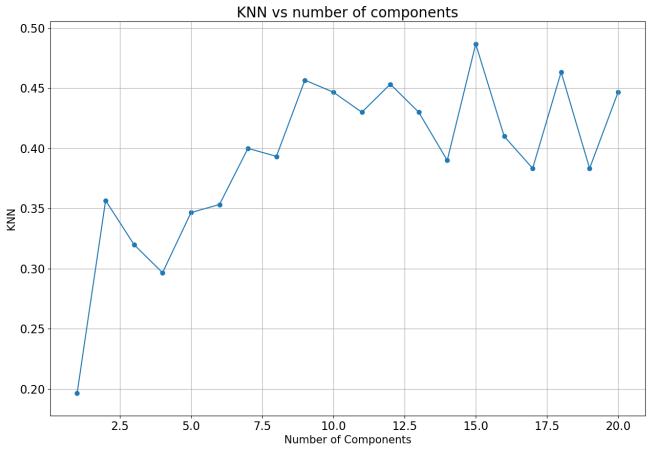

Figure 7: Average accuracy vs PCA dimensions using K-nearest neighbor classification

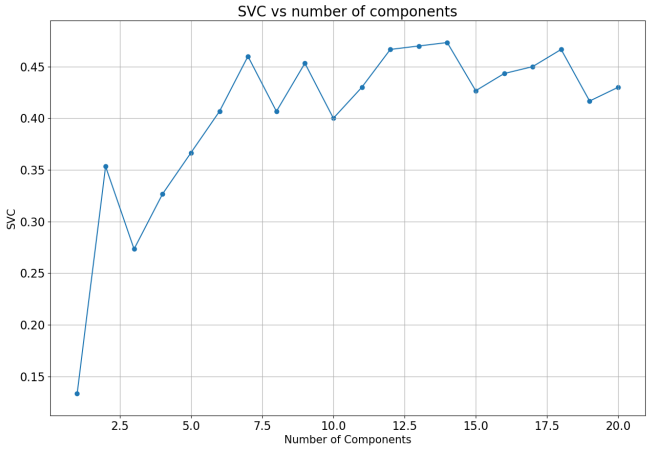

Figure 8: Average accuracy vs PCA dimensions using Support Vector Machine classification

of the information in the spectral data. Although 48.6% accuracy does not seem high at a glance, but using uniformly distributed random number between 1-20 gives an expected accuracy of 5%. Since we only used observations from 5 nights, we are able to improve the expected accuracy of the test data from 5% from a uniformly distributed answer to 48.6%.

We looked at the confusion matrix for the K-nearest neighbor classification to see which satellites get confused with one another. The confusion matrix is shown in Figure 9.

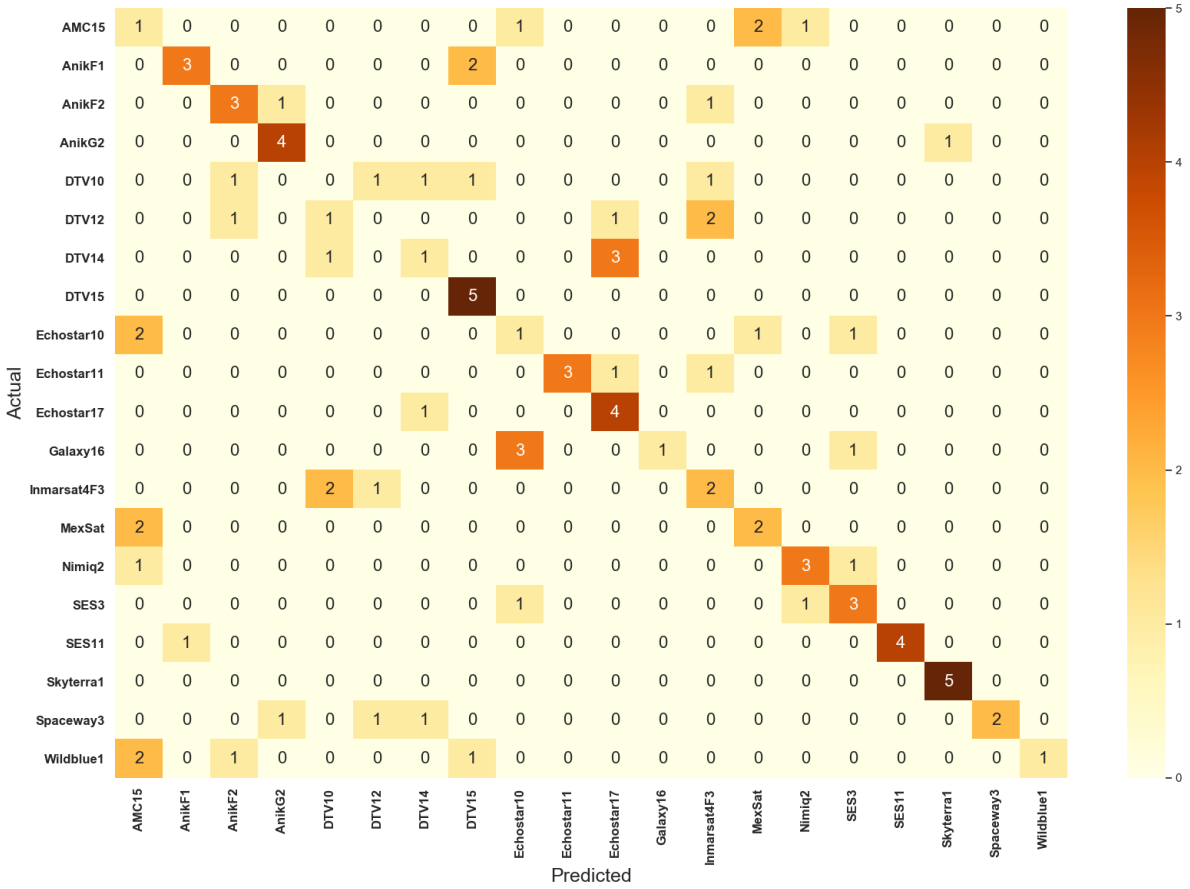

Figure 9: Confusing matrix for 20 satellites using 15 PCA components and 1 nearest neighbors

We see that there is a lot of confusion between DTV10, DTV12 and DTV14. It turns out that DTV10 and DTV12 have the same bus, so the confusion is reasonable. However, DTV14 has a different bus from DTV10 and DTV12. The classification model performed well for DTV15 and Skyterra1.

5.2 Classification of 20 satellites using limiting spectral resolution

The limited-resolution spectral signatures are also used to build a classification model. For this test we use the Optimizable Ensemble classifier. We allowed the classifier's hyperparam-

eters of 'NumLearningCycles', 'MaxNumSplits', 'LearnRate' and 'Method' to be Bayesian-optimized in MATLAB. To evaluate the classification accuracies, we use the cross-validation technique. Data is partitioned randomly into 60% training data and 40% test data, and an accuracy is calculated for the partition. The partitioning is repeated 10 times and the average accuracy is calculated and reported for the classifier. Figure 10 shows the confusion matrix of the classification model. The accuracy of 42.4% is comparable to the PCA-kNN results shown above. As mentioned, there are groups of satellites for which confusion is notable: the group of DTV10, DTV12 and DTV14 and the group of Echostar11 and Echostar17.

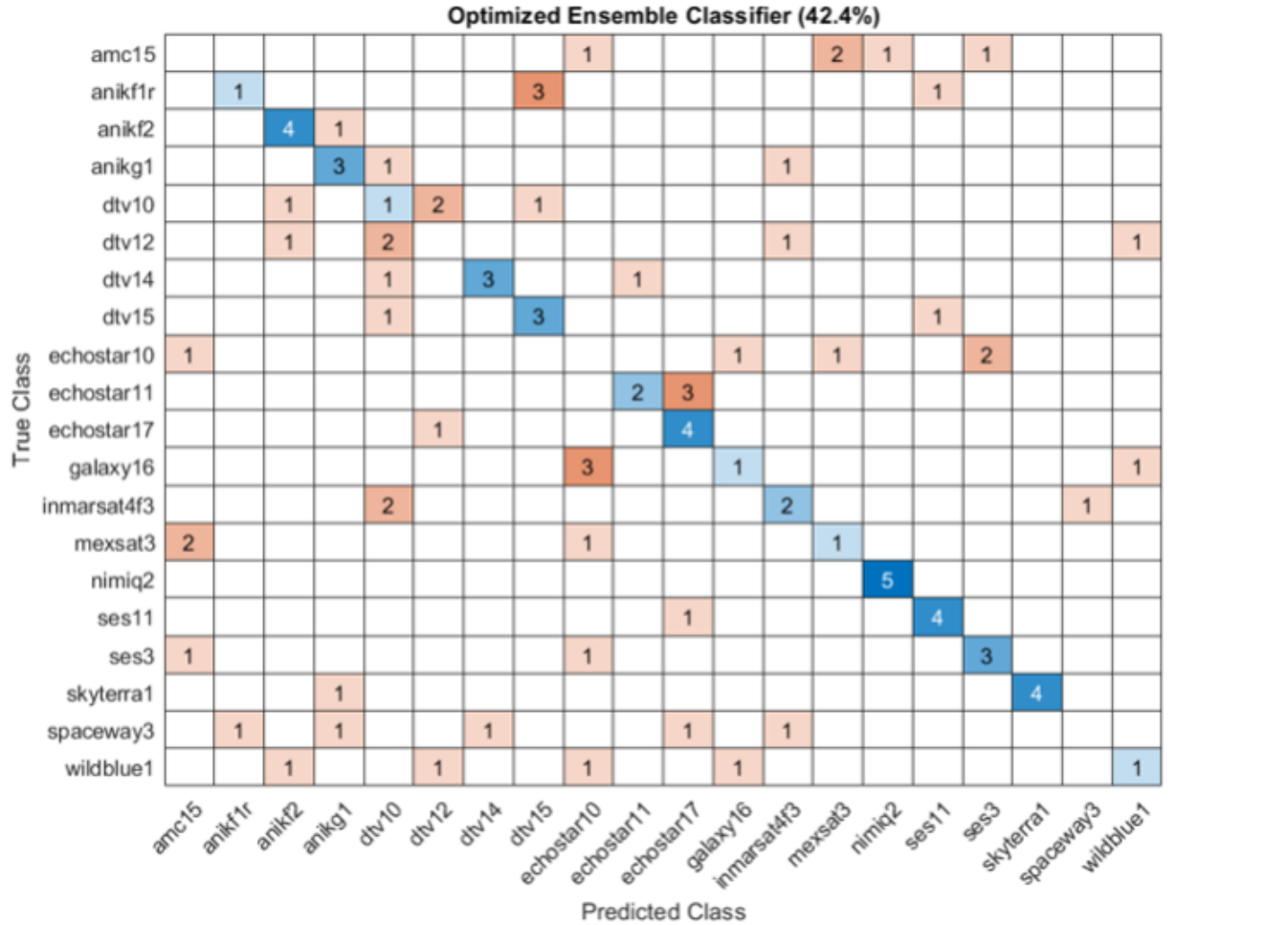

Figure 10: Confusion matrix for 20 satellites using the limited-resolution spectral signatures and the optimized Ensemble classifier.

5.3 Learning curve for classification of satellites

A learning curve is a great diagnostic tool for machine learning models. A learning curve is a plot where you plot the training accuracy and test accuracy as a function of training data size. Given a machine learning model, as you increase the training data size, you should expect the training accuracy to decrease and your test accuracy to increase. You can detect if your machine learning model is overfitting or underfitting using a learning curve. In addition, you can also see if you can improve your machine learning model accuracy by increasing the number of training data by looking at the slope of the learning curves. The learning curve for the K-nearest neighbor classification using 1 nearest-neighbor and 15 PCA dimensions is shown in Figure 11.

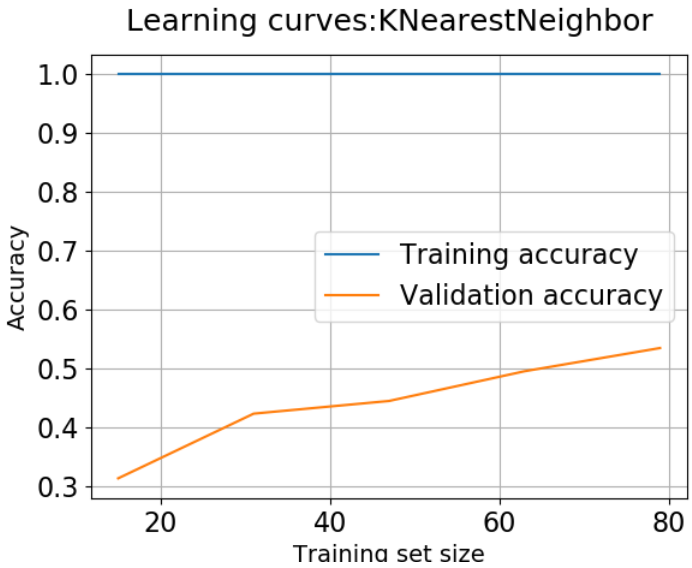

Figure 11: Learning curve for K-nearest neighbor classification using 1 nearest neighbors and 15 PCA components

We see that we have 100% accuracy on the training data, but the maximum validation accuracy is approximately 52%. The large gap between the training and validation curve shows that the training data is not a good representation of the validation data. Furthermore, the high training accuracy suggests that using 1-nearest neighbor for KNN might be overfitting the training data. To reduce the complex of the KNN model, we increase the number of

nearest neighbors to 2-nearest neighbors. The learning curve using 2-nearest neighbors at 15 PCA components is shown in Figure 12.

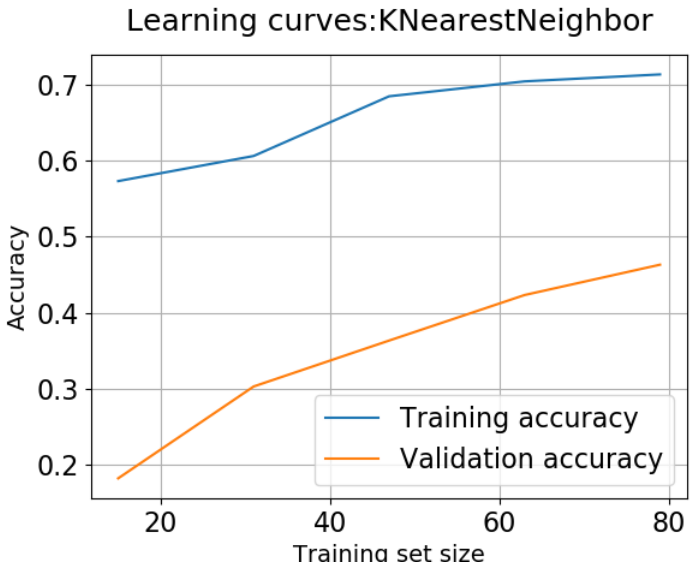

Figure 12: Learning curve for K-nearest neighbor classification using 2-nearest-neighbors and 15 PCA components

We see in Figure 12 that the training accuracy reduced significantly. However, the validation accuracy also reduced to approximately 47%.

Lastly, we can see from the slopes of the validation learning curves that our machine learning model can benefit drastically from more data.

6 Conclusion

In conclusion, we showed that using both PCA or limiting spectral resolution to reduce the dimension of the spectral data showed comparable accuracies. In addition, using different classification methods such as KNN, SVM or ensemble learning, the accuracies are also comparable. This shows that the limitation is not in the classification method, but in the data. This observable is also confirmed in the learning curve. Given the limited data (only 5 nights of collection), we were able to improve the classification accuracy from 5% (i.e.

uniformly distributed guess) to greater than 45%. We are confident that once we collect more data from future Glint seasons, we can improve our classification accuracy.

7 Acknowlegements

We want to acknowledge the support of the Air Force Office of Scientific Research, specifically the SDA Grand Challenge grant (20RT0930) under Dr. Erik Blasch (Program Officer for Dynamic Data and Information Processing)

8 Distribution Statement

9 Disclaimer

The views expressed in this article are those of the authors and do not necessarily reflect the official policy or position of the United States Air Force Academy, the United States Air Force, the United States Space Force, the Department of Defense, or the U.S. Government.

References

[1] P. D. Dao, X. C. Yee, D. M. Strong, B. Roth, and F. K. Chun. Multi-geosynchronous satellite classification with spectroscopic signatures. In Miguel Velez-Reyes and David W. Messinger, editors, *Algorithms, Technologies, and Applications for Multispectral and Hyperspectral Imaging XXIX*, volume 12519, page 1251907. International Society for Optics and Photonics, SPIE, 2023.

[2] F. Chun, R. Tippets, D. Strong, D. Della-Rose, D. Polsgrove, K. Gresham, J. Reid, C. Christy, M. Korbitz, J. Gray, S. Gartin, D. Coles, R. Haaland, R. Walker, J. Workman,

J. Mansur, V. Mansur, T. Hancock, J. Erdley, and E. Stoll. A new global array of optical telescopes: The falcon telescope network. *Publications of the Astronomical Society of the Pacific*, 130:095003, 07 2018.

[3] M. D. Parrish, J. A. Key, F. K. Chun, D. M. Strong, C. J. Wetterer, and P. Castro. Spectral analysis of unresolved satellite imagery. *Proceedings of SPIE: Algorithms, Technologies, and Applications for Multispectral and Hyperspectral Imaging*, 12094, 2022.

[4] K. F.R.S. Pearson. Liii. on lines and planes of closest fit to systems of points in space. *The London, Edinburgh, and Dublin Philosophical Magazine and Journal of Science*, 2(11):559–572, 1901.

[5] T. Cover and P. Hart. Nearest neighbor pattern classification. *IEEE Transactions on Information Theory*, 13(1):21–27, 1967.

[6] M.A. Hearst, S.T. Dumais, E. Osuna, J. Platt, and B. Scholkopf. Support vector machines. *IEEE Intelligent Systems and their Applications*, 13(4):18–28, 1998.